European Conference on Computational Fluid Dynamics
ECCOMAS CFD 2006
P. Wesseling, E. Oñate and J. Périaux (Eds)

A FINITE ELEMENT INTERIOR PENALTY METHOD FOR MHD IN HETEROGENEOUS DOMAINS

J.-L. Guermond[1,‡], R. Laguerre[1,2], J. Léorat[3], C. Nore[2,4]

[1]Department of Mathematics, Texas A&M University
3368 TAMU, College Station, TX 77843-3368, USA.
[2]Laboratoire d'Informatique pour la Mécanique et les Sciences de l'Ingénieur,
CNRS, BP 133, 91403 Orsay cedex, France.
[3]Luth, Observatoire de Paris-Meudon,
place Janssen, 92195-Meudon, France.
[4]Université Paris XI, Département de Physique, 91405 Orsay cedex, France.
[‡]On long leave from LIMSI (CNRS-UPR 3251), BP 133, 91403, Orsay, France.
guermond@math.tamu.edu, laguerre@limsi.fr, Jacques.Leorat@obspm.fr nore@limsi.fr

Key words: Finite elements, Discontinuous Galerkin, Magnetohydrodynamics, Dynamo action

Abstract. *The Maxwell equations in the MHD limit in heterogeneous domains composed of conducting and nonconducting regions are solved by using Lagrange finite elements and by enforcing continuities across interfaces using an interior penalty technique à la Nitsche/Dupont–Douglas [19, 8]. The method is shown to be stable and convergent and is validated by convergence tests. It is used to compute Ohmic decay in various compact conducting domains and to simulate the kinematic dynamo action in two different geometries.*

1 Introduction

The goal of the present report is to describe a finite element technique for solving the Maxwell equations in the MHD limit in heterogeneous domains. The main mathematical difficulties arising from this situation is that the magnetic field, $\mathbf{H}$, in the nonconducting region is curl free and the electric field, $\mathbf{E}$, cannot be eliminated by using the Ohm law in this region. Many methods have been proposed to solve this problem. One technique consists of modeling the insulating region as a weakly conducting one and eliminating $\mathbf{E}$ using the small artificial conductivity thereof, see e.g. [16]. This is a penalty method which is known to be ill-conditioned and not able to account for induced charge problems as found e.g. in the Faraday disk. Alternative algorithms involving vector potentials for the magnetic field or for the electric current have also been proposed (see for example [2, 9]). Another approach consists of realizing that $\mathbf{E}$ in the nonconducting region is the Lagrange multiplier associated with the constraint $\nabla\times\mathbf{H} = 0$, as emphasized in [13, 14]. It then

becomes clear that if both $\mathbf{E}$ and $\mathbf{H}$ are retained as dependent variables, the problem has a saddle point structure. If finite elements are used, this implies that either mixed pairs of finite elements (see e.g. [12, 13, 14]) or a stabilization method (e.g. Galerkin/Least-Squares, subgrid viscosity, Discontinuous Galerkin, etc.) must be employed. The former method has been shown to be efficient in two space dimensions in [12], but it turns out that retaining both $\mathbf{H}$ and $\mathbf{E}$ in the nonconducting region is somewhat computationally expensive in three space dimensions. This reason has led us to shift our focus on methods that are based on $\mathbf{H}$ in the conducting region and on a magnetic scalar potential in vacuum.

In fact, if the external insulating domain is simply connected, the magnetic field can be expressed in terms of an harmonic scalar potential ϕ. It is then possible to reduce the dynamical variables to $\mathbf{H}$ in the conducting region and to ϕ in the insulating exterior. A further reduction is possible in principle by using boundary elements to solve the external harmonic problem. This method has been introduced in [3] and shown in [15] to work well for solving the ohmic diffusion equation. However, it remains to be validated with the kinematic dynamo and the full nonlinear MHD equations, which is the focus of our group. If the boundary elements reduction alluded to above is not done, a serious question concerning the coupling of the two representations of the magnetic field arises. The tangential component of $\mathbf{H}$ must match the tangential component of $\nabla\phi$ across the interface between the conducting and nonconducting regions. Likewise, the normal component of $\mu^c\mathbf{H}$ must also match the normal component of $\mu^v\nabla\phi$ across this interface, where μ^c, μ^v are the magnetic permeabilities in the conducting and nonconducting regions respectively. As shown by Bossavit [4], it turns out that when using Nédélec finite elements (also called edge elements) the above coupling is natural. However, if Lagrange elements are used, this coupling becomes a serious mathematical headache. The first mathematical difficulty is that when strongly enforcing tangential boundary conditions on Lagrange elements, it may happen that a singular component of the solution is not computed if the interface is not smooth (see Costabel's Lemma [6][1]). Another issue is that exact coupling may sometimes be impossible when using polynomials to approximate $\mathbf{H}$ and ϕ. These reasons and the fact that we nevertheless insist on working with Lagrange elements have lead us to consider an interior penalty technique à la Nitsche/Dupont–Douglas [19, 8] to weakly enforce the coupling across the interface.

The method under consideration in the present paper consists of working with the pair $\mathbf{H}$–ϕ. In the conducting region we use Lagrange elements of degree $k \geq 1$ to approximate $\mathbf{H}$ and in the nonconducting region we use Lagrange elements of degree $k+1 \geq 2$ to approximate ϕ. The tangential component of the magnetic field is weakly enforced to be continuous across the interface by a consistent Interior Penalty method. The normal component of the magnetic induction is naturally (i.e., not particularly taken care of) enforced to be continuous across the interface by the weak formulation. The method

[1] $\mathbf{H}^1(\Omega)\cap\mathbf{H}_{0,\mathrm{curl}}(\Omega)$ is a genuine closed subspace of $\mathbf{H}_{0,\mathrm{curl}}(\Omega)\cap\mathbf{H}_{\mathrm{div}}(\Omega)$ if Ω is a non-convex polyhedron

is shown to be stable and convergent and is validated on three-dimensional benchmark problems.

The paper is organized as follows. We introduce the setting and a weak formulation of the problem under consideration in § 2. The interior penalty Galerkin approximation technique that we propose to solve the problem together with its stability and error analysis is presented in § 3. In § 4, we demonstrate the capability of the method by studying ohmic diffusion in different geometries and two examples of kinematic dynamo action. Concluding remarks are reported in Section 5.

2 The continuous problem

2.1 The setting

Let us consider the MHD limit of the Maxwell equations in a domain $\Omega \subset \mathbb{R}^3$:

$$\begin{cases} \mu \partial_t \mathbf{H} = -\nabla \times \mathbf{E}, \text{ in } \Omega \\ \nabla \times \mathbf{H} = \sigma(\mathbf{E} + \mathbf{u} \times \mu \mathbf{H}) + \mathbf{j}^s, \text{ in } \Omega \\ \mathbf{E} \times \mathbf{n}|_\Gamma = \mathbf{a}, \qquad \mathbf{H}|_{t=0} = \mathbf{H}_0, \end{cases} \tag{2.1}$$

where $\mathbf{j}^s$ is an externally imposed distribution of current, $\mathbf{u}$ an imposed velocity field, $\mathbf{a}$ a given boundary data, $\mathbf{H}_0$ an initial magnetic field, μ the permeability field, and σ the conductivity field. In the above formulation the displacement currents represented by the term $\epsilon \partial_t \mathbf{E}$ in the Ampère-Maxwell equation has been neglected due to the fact that $\mathbf{u}$ scales like L/T and the scales of interest L and T are such that $L/(\mathfrak{c}T)$ is extremely small (L, T and $\mathfrak{c}$ are the characteristic length scale, characteristic time scale, and speed of light, respectively).

Note also that this formulation is valid only if σ is uniformly positive over Ω and in this case an evolution equation for $\mathbf{H}$ can be obtained after eliminating the electric field. This short cut is no longer possible if σ vanishes in some sub-domains of Ω, and determining the complete solution, including the electric field, is no longer straightforward.

When σ is not uniformly positive, additional terms must be accounted for in (2.1) as we now explain. To be more specific, the domain is henceforth assumed to be bounded and its boundary Γ to be at least Lipschitz continuous. Ω is assumed to be partitioned into a conducting region (subscript c) and an insulating region (subscript v) as follows

$$\overline{\Omega} = \overline{\Omega}_c \cup \overline{\Omega}_v, \qquad \Omega_c \cap \Omega_v = \emptyset. \tag{2.2}$$

Ω_c is referred to as the conducting domain and Ω_v is referred to as the non-conducting domain. We henceforth assume that the conductivity $\sigma(\mathbf{x})$ is zero in Ω_v and is bounded from below and from above in Ω_c by positive constants, say σ_0 and σ_1, respectively. For instance the conducting medium occupying Ω_c could be the Earth core, the solar plasma, molten metals (gallium, sodium), or any other conducting material. The insulating region, Ω_v, could be for instance vacuum, the Earth mantle, or air. To refer to boundary

conditions easily, we introduce

$$\Gamma_c = \partial\Omega \cap \partial\Omega_c, \quad \Gamma_v = \partial\Omega \cap \partial\Omega_v, \quad \Gamma = \partial\Omega = \Gamma_v \cup \Gamma_c.$$

Moreover, we denote by Γ_v^0 the connected component of $\partial\Omega_v$ that contains Γ_v. We assume that $\partial\Omega_v$ has $J+1$ connected components, say

$$\Gamma_v^0, \Gamma_v^1, \ldots, \Gamma_v^J.$$

Figure 1 presents a particular setting with $J = 2$.

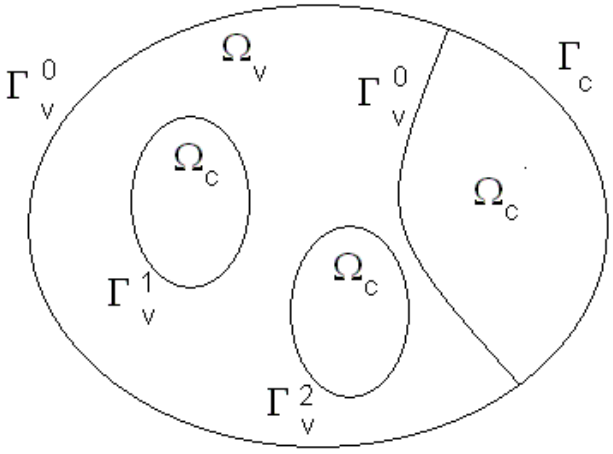

Figure 1: Computational domain with its different boundaries.

The interface between the conducting region and the nonconducting region is denoted by

$$\Sigma = \partial\Omega_c \cap \partial\Omega_v.$$

When σ and $\mathbf{j}^s$ are simultaneously zero somewhere in the domain, say in Ω_v, the problem (2.1) must be replaced by:

$$\begin{cases} \mu\partial_t \mathbf{H} = -\nabla\times\mathbf{E}, \text{ in } \Omega \\ \nabla\times\mathbf{H} = \begin{cases} \sigma(\mathbf{E} + \mathbf{u}\times\mu\mathbf{H}) + \mathbf{j}^s, & \text{in } \Omega_c \\ 0, & \text{in } \Omega_v \end{cases} \\ \nabla\cdot\mathbf{E} = 0, \text{ in } \Omega_v \\ \mathbf{E}\times\mathbf{n}|_\Gamma = \mathbf{a}, \qquad \mathbf{H}|_{t=0} = \mathbf{H}_0, \\ \displaystyle\int_{\Gamma_v^i} \mathbf{E}\cdot\mathbf{n} = 0, \quad 1 \le i \le J \end{cases} \tag{2.3}$$

where Γ_v^0, Γ_v^1, …, Γ_v^J are the $J+1$ connected components of $\partial\Omega_v$ as defined above. We refer to [4, 1] for more details on the asymptotic analysis leading to this model. Note

that the condition $\int_{\Gamma_v^0} \mathbf{E}\cdot\mathbf{n} = 0$ needs not be enforced since it is a consequence of the J other conditions together with $\mathbf{E}$ being solenoidal. Observe that the two extra conditions $\nabla\cdot\mathbf{E}|_{\Omega_v} = 0$ and $\int_{\Gamma_v^i} \mathbf{E}\cdot\mathbf{n} = 0$, $1 \le i \le J$ are what is left from the Ampère-Maxwell equation when passing to the limit to zero on the ratio $L/(\mathfrak{c}T)$ assuming that there is no electrostatic charge distributed in the domain. These extra conditions ensure that $\mathbf{E}$ is uniquely defined, i.e., they have no effect on $\mathbf{H}$.

2.2 Introduction of ϕ and elimination of E

If in addition to the above hypotheses on Ω, we assume that Ω_v is simply connected, the condition $\nabla\times\mathbf{H}|_{\Omega_v} = 0$ implies there is a scalar potential ϕ, defined up to an arbitrary constant, such that $\mathbf{H}|_{\Omega_v} = \nabla\phi$. Moreover, if the initial data $\mathbf{H}_0$ is such that $\nabla\times\mathbf{H}_0|_{\Omega_v} = 0$, we can also define ϕ_0 such that $\mathbf{H}_0|_{\Omega_v} = \nabla\phi_0$. By inserting the above definitions into (2.3) and by setting $\mathbf{E}^c = \mathbf{E}|_{\Omega_c}$, $\mathbf{E}^v = \mathbf{E}|_{\Omega_v}$, $\mathbf{H}^c = \mathbf{H}|_{\Omega_v}$, $\mu^c = \mu|_{\Omega_c}$, $\mu^v = \mu|_{\Omega_v}$, we infer that $\mathbf{H}^c$, $\mathbf{E}^c$, $\mathbf{E}^v$, ϕ solve

$$\begin{cases} \mu^c\partial_t\mathbf{H}^c = -\nabla\times\mathbf{E}^c, & \nabla\times\mathbf{H}^c = \sigma(\mathbf{E}^c + \mathbf{u}\times\mu^c\mathbf{H}^c) + \mathbf{j}^s, & \text{in } \Omega_c \\ \mu^v\partial_t\nabla\phi = -\nabla\times\mathbf{E}^v, & \nabla\cdot\mathbf{E}^v = 0 & \text{in } \Omega_v \\ \mathbf{H}^c\times\mathbf{n}^c + \nabla\phi\times\mathbf{n}^v = 0 & \mathbf{E}^c\times\mathbf{n}^c + \mathbf{E}^v\times\mathbf{n}^v = 0 & \text{on } \Sigma \\ \mathbf{E}^c\times\mathbf{n}^c|_{\Gamma_c} = \mathbf{a} & \mathbf{E}^v\times\mathbf{n}^v|_{\Gamma_v} = \mathbf{a}, & \\ \int_{\Gamma_v^i}\mathbf{E}\cdot\mathbf{n} = 0, & 1 \le i \le J & \\ \mathbf{H}^c|_{t=0} = \mathbf{H}_0^c, & \phi|_{t=0} = \phi_0. & \end{cases} \tag{2.4}$$

Note that the condition $(\mathbf{H}^c\times\mathbf{n}^c + \nabla\phi\times\mathbf{n}^v)|_\Sigma = 0$ is meant to ensure that the curl of the field

$$\mathbf{H} = \begin{cases} \mathbf{H}^c & \text{in } \Omega_c \\ \nabla\phi & \text{in } \Omega_v \end{cases}$$

has no singular measure concentrated on Σ. The analogous condition $(\mathbf{E}^c\times\mathbf{n}^c + \mathbf{E}^v\times\mathbf{n}^v)|_\Sigma = 0$ ensures the same property for the curl of $\mathbf{E}$.

The arbitrariness of ϕ up to a constant can be removed by enforcing ϕ to be of zero mean, say $\int_{\Omega_v}\phi = 0$.

Assuming enough regularity is at hand, we now formally eliminate $\mathbf{E}$ by proceeding as follows: we use Ohm's law to eliminate $\mathbf{E}^c$ from Faraday's equation in the conducting region. We take the divergence of Faraday's equation in the nonconducting medium to get rid of $\nabla\times\mathbf{E}^v$. We eliminate the tangential component of $\mathbf{E}$ on Γ_v by using the following

representation $\mathbf{E}^v|_{\Gamma_v} = (\mathbf{E}^v\cdot\mathbf{n}^v)\mathbf{n}^v + \mathbf{n}^v\times\mathbf{a}$. Finally we obtain:

$$\begin{cases} \mu^c\partial_t\mathbf{H}^c = -\nabla\times(\frac{1}{\sigma}(\nabla\times\mathbf{H}^c - \mathbf{j}^s) - \mathbf{u}\times\mu^c\mathbf{H}^c), & \text{in } \Omega_c \\ \mu^v\partial_t\Delta\phi = 0 & \text{in } \Omega_v \\ (\nabla\times\mathbf{H}^c - \sigma\mathbf{u}\times\mu\mathbf{H}^c)\times\mathbf{n}^c = \sigma\mathbf{a} + \mathbf{j}^s\times\mathbf{n}^c & \text{on } \Gamma_c \\ \mu^v\partial_{\mathbf{n}^v}(\partial_t\phi) = -\mathbf{n}^v\cdot\nabla\times(\mathbf{n}^v\times\mathbf{a}), & \text{on } \Gamma_v \\ \mathbf{H}^c\times\mathbf{n}^c + \nabla\phi\times\mathbf{n}^v = 0 & \text{on } \Sigma \\ \mu^c\mathbf{H}^c\cdot\mathbf{n}^c + \mu^v\nabla\phi\cdot\mathbf{n}^v = 0 & \text{on } \Sigma \\ \mathbf{H}^c|_{t=0} = \mathbf{H}_0^c, \qquad \phi|_{t=0} = \phi_0. \end{cases} \tag{2.5}$$

Observe that the operator $\mathbf{n}^v\cdot\nabla\times(\cdot)$ involves only tangential derivatives; hence, it is meaningful to have it acting on the field $\mathbf{n}^v\times\mathbf{a}$ which is only defined on Γ. Note also that $(\mu^c\mathbf{H}^c\cdot\mathbf{n}^c + \mu^v\nabla\phi\cdot\mathbf{n}^v)|_\Sigma = 0$ express the continuity of the normal component of the magnetic induction across Σ. This equation is a consequence of the continuity of the tangential component of the electric field. If the electric field is needed, it is computed in the conducting domain by using Ohm's law, and it is determined in the nonconducting medium by solving the Cauchy-Riemann problem: $\nabla\times\mathbf{E}^v = -\mu^v\partial_t\nabla\phi$, $\nabla\cdot\mathbf{E}^v = 0$, $\mathbf{E}^v\times\mathbf{n}^v|_\Sigma = -\mathbf{E}^c\times\mathbf{n}^c|_\Sigma$, $\mathbf{E}^v\times\mathbf{n}|_\Gamma = \mathbf{a}$, and $\int_{\Gamma_v^i}\mathbf{E}^v\cdot\mathbf{n} = 0$, $1\le i\le J$.

2.3 Weak formulation

Let us now construct a weak formulation for Problem (2.5). We henceforth assume that $\mathbf{u}\in L^\infty(0,+\infty;\mathbf{L}^2(\Omega_c))$ and $\mathbf{j}^s\in L^\infty(0,+\infty;\mathbf{L}^2(\Omega_c))$, where $L^p(0,+\infty;E)$ is the set of the functions that map the time interval $(0,+\infty)$ to the normed space E and whose norm in E is L^p integrable, $1\le p\le+\infty$. Likewise we assume that σ and μ^c are both in $L^\infty(0,+\infty;L^\infty(\Omega_c))$ and μ^v is in $L^\infty(0,+\infty;L^\infty(\Omega_v))$. To alleviate notation, we use the notation $(\mathbf{f},\mathbf{g})_E$ to denote the integral $\int_E\mathbf{f}\cdot\mathbf{g}$, where E is any measurable subset of Ω or $\Gamma_v\cup\Gamma_c$.

Instead of working directly with (2.5) it turns out that it is more straightforward to construct the weak formulation starting from (2.4) and eliminating $\mathbf{E}$ on the fly. Let $\mathbf{b}\in\mathbf{H}_{\text{curl}}(\Omega_c)$ be a test function. After multiplying the Faraday equation by $\mathbf{b}$ in Ω_c in (2.4), integrating over Ω_c, and integrating by parts, we obtain

$$(\mu^c\partial_t\mathbf{H}^c,\mathbf{b})_{\Omega_c} + (\mathbf{E}^c,\nabla\times\mathbf{b})_{\Omega_c} + (\mathbf{E}^c,\mathbf{b}\times\mathbf{n}^c)_\Sigma = (\mathbf{E}^c\times\mathbf{n}^c,\mathbf{b})_{\Gamma_c}.$$

Then using Ohm's law in Ω_c and using the boundary conditions on $\mathbf{E}^c$ yields

$$\begin{aligned}(\mu^c\partial_t\mathbf{H}^c,\mathbf{b})_{\Omega_c} + (\tfrac{1}{\sigma}\nabla\times\mathbf{H}^c,\nabla\times\mathbf{b})_{\Omega_c} + (\tfrac{1}{\sigma}\nabla\times\mathbf{H}^c,\mathbf{b}\times\mathbf{n}^c)_\Sigma \\ = (\tfrac{1}{\sigma}\mathbf{j}^s + \mathbf{u}\times\mu^c\mathbf{H}^c,\nabla\times\mathbf{b})_{\Omega_c} + (\tfrac{1}{\sigma}\mathbf{j}^s + \mathbf{u}\times\mu^c\mathbf{H}^c,\mathbf{b}\times\mathbf{n}^c)_\Sigma + (\mathbf{a},\mathbf{b})_{\Gamma_c}.\end{aligned} \tag{2.6}$$

Likewise by using $\nabla\psi$, $\psi\in H^1(\Omega_v)$, to test the Faraday equation in Ω_v in (2.4), we obtain

$$(\mu^v\partial_t\nabla\phi,\nabla\psi)_{\Omega_v} - (\mathbf{E}^v\times\mathbf{n}^v,\nabla\psi)_\Sigma = (\mathbf{E}^c\times\mathbf{n}^c,\nabla\psi)_{\Gamma_v}.$$

By using again the boundary condition together with the fact that

$$\mathbf{E}^v\times\mathbf{n}^v|_\Sigma = -\mathbf{E}^c\times\mathbf{n}^c|_\Sigma = -(\tfrac{1}{\sigma}(\nabla\times\mathbf{H}^c - \mathbf{j}^s) - \mathbf{u}\times\mu^c\mathbf{H}^c)\times\mathbf{n}^c|_\Sigma,$$

we infer

$$(\mu^v\partial_t\nabla\phi, \nabla\psi)_{\Omega_v} + (\tfrac{1}{\sigma}(\nabla\times\mathbf{H}^c - \mathbf{j}^s) - \mathbf{u}\times\mu^c\mathbf{H}^c, \nabla\psi\times\mathbf{n}^v)_\Sigma = (\mathbf{a}, \nabla\psi)_{\Gamma_v}. \tag{2.7}$$

For the above developments to make sense we now specify the regularity we expect to hold on $\mathbf{H}^c$ and ϕ by introducing

$$\mathbf{L} = \{(\mathbf{b},\psi) \in \mathbf{L}^2(\Omega_c)\times H^1_{\int=0}(\Omega_v)\}, \tag{2.8}$$

$$\mathbf{X} = \{(\mathbf{b},\psi) \in \mathbf{H}_{\mathrm{curl}}(\Omega_c)\times H^1_{\int=0}(\Omega_v);\ (\mathbf{b}\times\mathbf{n}^c + \nabla\psi\times\mathbf{n}^v)|_\Sigma = 0\}, \tag{2.9}$$

and we equip $\mathbf{L}$ and $\mathbf{X}$ with the norm of $\mathbf{L}^2(\Omega_c)\times H^1(\Omega_v)$ and $\mathbf{H}_{\mathrm{curl}}(\Omega_c)\times H^1(\Omega_v)$, respectively. Here, $H^1_{\int=0}(\Omega_v)$ is the subspace of $H^1(\Omega_v)$ composed of the functions of zero mean value. Recall that owing to the Poincaré–Friedrichs inequality $\|\nabla\phi\|_{L^2(\Omega_v)}$ is a norm equivalent to that of $H^1(\Omega_v)$.

By adding (2.6) and (2.7) we obtain that the pair $(\mathbf{H}^c,\phi)$ solves

$$\begin{aligned}(\mu^c\partial_t\mathbf{H}^c, \mathbf{b})_{\Omega_c} + (\mu^v\partial_t\nabla\phi, \nabla\psi)_{\Omega_v} + (\tfrac{1}{\sigma}(\nabla\times\mathbf{H}^c - \mathbf{j}^s) - \mathbf{u}\times\mu^c\mathbf{H}^c, \nabla\times\mathbf{b})_{\Omega_c}\\ + (\tfrac{1}{\sigma}(\nabla\times\mathbf{H}^c - \mathbf{j}^s) - \mathbf{u}\times\mu^c\mathbf{H}^c, \mathbf{b}\times\mathbf{n}^c + \nabla\psi\times\mathbf{n}^v)_\Sigma = (\mathbf{a},\mathbf{b})_{\Gamma_c} + (\mathbf{a},\nabla\psi)_{\Gamma_v}.\end{aligned} \tag{2.10}$$

Observe that the term $(\frac{1}{\sigma}(\nabla\times\mathbf{H}^c - \mathbf{j}^s) - \mathbf{u}\times\mu^c\mathbf{H}^c, \mathbf{b}\times\mathbf{n}^c + \nabla\psi\times\mathbf{n}^v)_\Sigma$ is zero whenever the pair of test functions $(\mathbf{b},\psi)$ is a member of $\mathbf{X}$. This term will play a major role when it comes to constructing a nonconforming approximation to the problem, see §3.1.

We are now in measure to formulate the problem as follows: Seek the pair $(\mathbf{H}^c,\phi) \in L^2(0,+\infty;\mathbf{X})\cap L^\infty(0,+\infty,\mathbf{L})$ with $(\partial_t\mathbf{H}^c, \partial_t\phi) \in L^2(0,+\infty;\mathbf{X}')$ such that for all $(\mathbf{b},\psi) \in X$ and a.e. $t \in (0,+\infty)$,

$$\begin{cases}\mathbf{H}^c|_{t=0} = \mathbf{H}^c_0; \quad \nabla\phi|_{t=0} = \nabla\phi_0,\\ (\mu^v\partial_t\mathbf{H}^c, b)_{\Omega_c} + (\mu^v\partial_t\nabla\phi,\nabla\psi)_{\Omega_v} + (\tfrac{1}{\sigma}\nabla\times\mathbf{H}^c - \mathbf{u}\times\mu^c\mathbf{H}^c, \nabla\times\mathbf{b})_{\Omega_c}\\ \qquad\qquad = (\tfrac{1}{\sigma}\mathbf{j}^s, \nabla\times\mathbf{b})_{\Omega_c} + (\mathbf{a},\mathbf{b})_{\Gamma_c} + (\mathbf{a},\nabla\psi)_{\Gamma_v}.\end{cases} \tag{2.11}$$

To alleviate notation, let us define the following bilinear form

$$a((\mathbf{b},\psi),(\mathbf{h},\varphi)) = (\tfrac{1}{\sigma}\nabla\times\mathbf{b} - \mathbf{u}\times\mu^c\mathbf{b}, \nabla\times\mathbf{h})_{\Omega_c}, \quad \forall(\mathbf{b},\psi),(\mathbf{h},\varphi) \in X. \tag{2.12}$$

Theorem 2.1. *The problem (2.11) is wellposed.*

2.4 Stabilized weak formulation

It is clear from (2.4) that if $\mathbf{H}_0^c$ is solenoidal, $\mathbf{H}^c$ stays solenoidal for all times. Note however, that $\nabla\cdot\mathbf{H}^c = 0$ is not part of the system defining the magnetic field but is merely a consequence of Faraday's equation. Nevertheless, provided $\nabla\cdot\mathbf{H}_0^c = 0$, it is quite common to transform $\nabla\cdot\mathbf{H}^c = 0$ into a constraint by replacing Faraday's equation in Ω_c in (2.4) by

$$\mu^c\partial_t\mathbf{H}^c = -\nabla\times\mathbf{E}^c + \nabla(\alpha\nabla\cdot\mu^c\mathbf{H}^c), \tag{2.13}$$

$$\nabla\cdot(\mu^c\mathbf{H}^c)|_{\Gamma_c} = 0, \tag{2.14}$$

where $\alpha = \alpha(x)$ is a user-defined scalar-valued function (a constant may do the job), which must be positive, uniformly bounded from above, uniformly bounded away from zero from below, and should be chosen so that the magnitude of the two terms in the right-hand side are balanced. Henceforth we assume $\alpha(x) \geq \alpha_0 > 0$ for all $x \in \Omega_c$. Consequently, without any additional difficulty, we shall henceforth consider a modified (i.e., stabilized) version of the problem (2.11) by replacing the bilinear form a by the following one

$$\tilde{a}((\mathbf{b},\psi),(\mathbf{h},\varphi)) = a((\mathbf{b},\psi),(\mathbf{h},\varphi)) + (\alpha\nabla\cdot\mu^c\mathbf{b}, \nabla\cdot\mu^c\mathbf{h})_{\Omega_c}. \tag{2.15}$$

3 Finite element approximation

We now approximate the problem (2.11) by using finite elements. The key feature of the method that we propose is that the continuity of the tangential component of the magnetic field across Σ is enforced weakly by using an interior penalty technique. This technique is the work horse of Discontinuous Galerkin approximation methods for elliptic and parabolic equations [8].

3.1 The Interior Penalty Galerkin approximation

Let $\{\mathcal{T}_h^c\}_{h>0}$ and $\{\mathcal{T}_h^v\}_{h>0}$ be regular families of non-overlapping meshes for Ω_c and Ω_v, respectively. For the sake of simplicity we assume that the meshes are composed of simplices and the interface between the two non-overlapping meshes $\mathcal{T}_h^c$ and $\mathcal{T}_h^v$ is Σ. Let k be a positive integer. The approximation space for the magnetic field and the scalar potential is denoted by $\mathbf{X}_h = \mathbf{X}_h^{\mathbf{H}}\times X_h^{\phi}$ and defined as follows

$$\mathbf{X}_h = \{(\mathbf{b},\psi) \in \boldsymbol{\mathcal{C}}^0(\overline{\Omega_c})\times\mathcal{C}^0(\overline{\Omega_v});\ \mathbf{b}|_K \in \mathbb{P}_k,\ \forall K \in \mathcal{T}_h^c;\ \psi|_K \in \mathbb{P}_{k'},\ \forall K \in \mathcal{T}_h^v\}. \tag{3.1}$$

We shall also use the space $\mathbf{X}_{(h)} = [\mathbf{H}^1(\Omega_c)\times H^2(\Omega_v)]+\mathbf{X}_h$. Observe that for any given pair $(\mathbf{b},\psi)$ in $\mathbf{X}_h$ we do not enforce the tangent component of $\mathbf{b}$ to match that of the gradient of ψ across Σ. Actually, enforcing such a match would be impossible in most practical situations unless $\mathbf{X}_h$ is composed of the so-called edge elements or Nédélec elements. Since we do not want to use edge elements, the matching in question will be enforced weakly as explained below.

Since the solution to (2.11) also satisfies (2.10) where the test functions $\mathbf{b}$ and ψ may be discontinuous, we define the following bilinear form on $\mathbf{X}_{(h)}\times\mathbf{X}_h$:

$$a_h((\mathbf{h},\varphi),(\mathbf{b},\psi)) = \tilde{a}((\mathbf{h},\varphi),(\mathbf{b},\psi)) + (\tfrac{1}{\sigma}\nabla\times\mathbf{h} - \mathbf{u}\times\mu\mathbf{h}, (\mathbf{b}\times\mathbf{n}^c + \nabla\psi\times\mathbf{n}^v))_\Sigma + \beta(\tfrac{1}{h}(\mathbf{h}\times\mathbf{n}^c + \nabla\varphi\times\mathbf{n}^v), (\mathbf{b}\times\mathbf{n}^c + \nabla\psi\times\mathbf{n}^v))_\Sigma. \quad (3.2)$$

The parameter $\beta > 0$ is a tunable constant and h denotes the typical mesh size. The second term in the right-hand side of (3.2) is the consistency term already present in (2.10). As already mentioned earlier, this term vanishes whenever $\mathbf{b}\times\mathbf{n}^c + \nabla\psi\times\mathbf{n}^v$ is zero on Σ. The last term is a penalty term. It is meant to constrain the jump of the tangential component of the approximate magnetic field across Σ to be small.

Let $[0,T]$ be some given time interval. Let $\mathbf{H}^c_{0,h} \in \mathbf{X}_h$ and $\phi_{0,h} \in M_h$ be approximations of $\mathbf{H}^c_0$ and ϕ_0, respectively. The semi-discrete problem is formulated as follows: Seek $(\mathbf{H}^c_h, \phi_h) \in \mathcal{C}^1([0,T];\mathbf{X}_h)$ such that for all $(\mathbf{b},\psi) \in \mathbf{X}_h$ and all $t \in [0,T]$,

$$\begin{cases} (\mathbf{H}^c_h, \phi_h)|_{t=0} = (\mathbf{H}^c_{0,h}, \phi_{0,h}), \\ (\mu^c\partial_t\mathbf{H}_h, \mathbf{b})_{\Omega_c} + (\mu^v\nabla\partial_t\phi_h, \nabla\psi)_{\Omega_v} + a_h((\mathbf{H}^c_h,\phi_h),(\mathbf{b},\psi)) = J((\mathbf{H}^c_h,\phi_h),(\mathbf{b},\psi)), \end{cases} \quad (3.3)$$

where the source term is given by

$$J((\mathbf{H}^c_h,\phi_h),(\mathbf{b},\psi)) = (\tfrac{1}{\sigma}\mathbf{j}^s, \nabla\times\mathbf{b})_{\Omega_c} + (\tfrac{1}{\sigma}\mathbf{j}^s, \mathbf{b}\times\mathbf{n}^c + \nabla\psi\times\mathbf{n}^v)_\Sigma + (\mathbf{a},\mathbf{b})_{\Gamma_c} + (\mathbf{a},\nabla\psi)_{\Gamma_v}, \quad (3.4)$$

The error analysis will show that β must be taken large enough for the method to be convergent. This feature is characteristic of Interior Penalty methods. It would have been possible to overcome this slight inconvenience by using a Local Discontinuous Galerkin (LDG) approach, [5, 20]. We preferred not using this approach since LDG requires solving local problems.

3.2 Error analysis

We perform the error analysis of problem (3.3) in this section.

Before stating the main convergence result, we define appropriate interpolation operators. For all $\mathbf{H}^c \in \mathcal{C}^1(0,T;\mathbf{H}^1(\Omega_c))$ we define $\boldsymbol{\pi}_h\mathbf{H}^c \in \mathcal{C}^1(0,T;\mathbf{X}^{\mathbf{H}}_h)$ so that $\boldsymbol{\pi}_h\mathbf{H}^c|_{t=0} = \boldsymbol{\mathcal{I}}_h\mathbf{H}^c|_{t=0}$ where $\boldsymbol{\mathcal{I}}_h$ is an interpolation operator with optimal interpolation properties (e.g. Lagrange, Clément, or Scott-Zhang interpolation operators.), and for all $\mathbf{b} \in \mathbf{X}^{\mathbf{H}}_h$ and for a.e. $t \in (0,T)$,

$$(\mu^c\partial_t\boldsymbol{\pi}_h\mathbf{H}^c,\mathbf{b})_{\Omega_c} + (\tfrac{1}{\sigma}\nabla\times\boldsymbol{\pi}_h\mathbf{H}^c, \nabla\times\mathbf{b})_{\Omega_c} + (\alpha\nabla\cdot(\mu^c\boldsymbol{\pi}_h\mathbf{H}^c), \nabla\cdot(\mu^c\mathbf{b}))_{\Omega_c} = (\mu^c\partial_t\mathbf{H}^c,\mathbf{b})_{\Omega_c} + (\tfrac{1}{\sigma}\nabla\times\mathbf{H}^c, \nabla\times\mathbf{b})_{\Omega_c} + (\alpha\nabla\cdot(\mu^c\mathbf{H}^c), \nabla\cdot(\mu^c\mathbf{b}))_{\Omega_c}. \quad (3.5)$$

We henceforth assume that the following approximation result holds: There are $k_1 \geq k_2 > 0$ such that

$$\|\boldsymbol{\pi}_h\mathbf{H}^c - \mathbf{H}^c\|_{L^\infty(0,T;\mathbf{L}^2(\Omega_c))} + \|(\boldsymbol{\pi}_h\mathbf{H}^c - \mathbf{H}^c)\times\mathbf{n}^c\|_{L^2(0,T;\mathbf{L}^2(\Sigma))} \leq ch^{k_1}\|\mathbf{H}^c\|_{\mathbf{Ho}} \quad (3.6)$$

$$\|\nabla\times(\boldsymbol{\pi}_h\mathbf{H}^c-\mathbf{H}^c)\|_{L^2(0,T;\mathbf{L}^2(\Omega_c))}+\|\nabla\cdot(\boldsymbol{\pi}_h\mathbf{H}^c-\mathbf{H}^c)\|_{L^2(0,T;\mathbf{L}^2(\Omega_c))}$$
$$+\|\nabla\times(\boldsymbol{\pi}_h\mathbf{H}^c-\mathbf{H}^c)\times\mathbf{n}^c\|_{L^2(0,T;\mathbf{L}^2(\Sigma))}\le ch^{k_2}\|\mathbf{H}^c\|_{\mathbf{Ho}},\quad(3.7)$$

where $\|\cdot\|_{\mathbf{Ho}}$ is a norm involving high-order space derivatives, for instance $\|\mathbf{H}^c\|_{\mathbf{Ho}}=\|\mathbf{H}^c\|_{L^\infty(0,T;\mathbf{W}^{k_1+1,\infty}(\Omega_c))}$. Proving these estimates (the first one in (3.6) and the first and second one in (3.7)) for $k_1=k_2=k$ is a standard exercise. Proving $k_1=k+1$ for the second term in (3.6) and $k_2=k$ for the third term in (3.7) is not trivial and is far beyond the scope of the present paper. If all the possible regularity is at hand, we should expect $k_1=k+1$ and $k_2=k$.

We also define an interpolation operator for scalar potentials. For all $\phi\in\mathcal{C}^1(0,T;\mathbf{H}^1(\Omega_v))$ we define $\pi_h\phi\in\mathcal{C}^1(0,T;\mathbf{X}_h^\phi)$ so that for all $\psi\in\mathbf{X}_h^\phi$ and for a.e. $t\in(0,T)$,

$$(\mu^v\nabla\pi_h\phi,\nabla\psi)_{\Omega_v}=(\mu^v\nabla\phi,\nabla\psi)_{\Omega_v}.\quad(3.8)$$

Likewise, we assume that the following error estimates hold: There is $\ell>0$ such that

$$\|\nabla(\pi_h\phi-\phi)\|_{L^\infty(0,T;\mathbf{L}^2(\Omega_v))}+\|\nabla(\pi_h\phi-\phi)\times\mathbf{n}^c\|_{L^2(0,T;\mathbf{L}^2(\Sigma))}\le ch^\ell\|\phi\|_{\mathrm{Ho}}.\quad(3.9)$$

When maximal regularity is at hand, it is a standard exercise to prove $\ell=k'$ for the first term in the left-hand side. Proving $\ell=k'$ for the second term is far more technical and relies on $W^{1,\infty}$ estimates.

We finally assume that the algorithm is initialized so that

$$\|\mathbf{H}_0-\mathbf{H}_{0,h}^c\|_{\mathbf{L}^2(\Omega_c)}\le c\,h^{k_1}\|\mathbf{H}^c\|_{\mathbf{Ho}},\qquad\|\phi_0-\phi_{0,h}\|_{\mathbf{L}^2(\Omega_v)}\le c\,h^\ell\|\phi\|_{\mathrm{Ho}}.\quad(3.10)$$

Having introduced k_1, k_2, and ℓ, we are now in measure to state the convergence result.

Theorem 3.1. *Under the above assumptions and provided the solution to (2.11) is smooth enough (say $|\mathbf{H}^c\|_{\mathbf{Ho}}$ and $\|\phi\|_{\mathrm{Ho}}$ finite) and β is large enough, the solution to (3.3) satisfies the following error estimates*

$$\|\mathbf{H}^c-\mathbf{H}_h^c\|_{L^\infty(0,T;\mathbf{L}^2(\Omega_c))}+\|\phi-\phi_h\|_{L^\infty(0,T;H^1(\Omega_v))}\le ch^{\min(k_1-\frac12,k_2+\frac12,\ell-\frac12)}\quad(3.11)$$

$$\|\nabla\times(\mathbf{H}^c-\mathbf{H}_h^c)\|_{L^2(0,T;\mathbf{L}^2(\Omega_c))}+\|\nabla\cdot\mathbf{H}_h^c\|_{L^2(0,T;\mathbf{L}^2(\Omega_c))}\le ch^{\min(k_1-\frac12,k_2,\ell-\frac12)}\quad(3.12)$$

If full regularity is at hand $k_1=k+1$, $k_2=k$, and $\ell=k'$, The above result yields $\|\mathbf{H}^c-\mathbf{H}_h^c\|_{\mathbf{L}^2(\Omega_c)}\le ch^{\min(k+\frac12,k'-\frac12)}$. This in turn shows that to obtain optimality we should take

$$k'=k+1,\quad(3.13)$$

i.e., the finite elements used to approximate the scalar potential are one degree higher than those used to approximate the magnetic filed in Ω_c. This is coherent with the fact that the magnetic field in Ω_v is the gradient of ϕ, i.e., the magnetic field is deduced from ϕ by derivation. In conclusion, if we set $k'=k+1$ and if full regularity is guaranteed, the above theorem yields

$$\|\mathbf{H}^c-\mathbf{H}_h^c\|_{L^\infty(0,T;\mathbf{L}^2(\Omega_c))}+\|\phi-\phi_h\|_{L^\infty(0,T;H^1(\Omega_v))}\le ch^{k+\frac12}\quad(3.14)$$

$$\|\nabla\times(\mathbf{H}^c-\mathbf{H}_h^c)\|_{L^2(0,T;\mathbf{L}^2(\Omega_c))}+\|\nabla\cdot\mathbf{H}_h^c\|_{L^2(0,T;\mathbf{L}^2(\Omega_c))}\le ch^k\quad(3.15)$$

These estimates are confirmed by the numerical tests reported elswhere [11].

4 Applications

We report in this section tests that we made to validate our code in three dimensions. In this entire section μ is assumed to be constant and $\mu^c = \mu^v$. The domains Ω_c and Ω_v being axisymmetric, we use finite elements in the meridian plane and Fourier expansion in the azimuthal direction. For instance, the approximate scalar potential is decomposed as follows:

$$\phi_h(r,\theta,z,t) = \phi^c_{h,0}(r,z,t) + \sum_{m=1}^{M} \phi^c_{h,m}(r,z,t)\cos(m\theta) + \phi^s_{h,m}(r,z,t)\sin(m\theta),$$

where $\phi^c_{h,0}$, $\phi^c_{h,m}$, and $\phi^s_{h,m}$ are time-dependent two-dimensional finite element functions. The same decomposition is used for the approximate magnetic field. All the computations reported in this section have been done using $\mathbb{P}_1$ finite elements in the conducting region and $\mathbb{P}_2$ finite elements in the non-conducting region.

4.1 Ohmic decay in a compact conducting domain

We set the velocity field to zero and we assume that μ and σ are constants. The MHD equations (2.5) then reduce to the vector heat equation in the conducting region for $\mathbf{H}^c$ and to the Laplace equation in the nonconducting region for the scalar potential:

$$\begin{cases} \partial_t \mathbf{H}^c = \Delta \mathbf{H}^c, \text{ in } \Omega_c \\ \Delta \partial_t \phi = 0, \text{ in } \Omega_v, \qquad \phi \to 0 \text{ at infinity}, \\ \mathbf{H}^c|_\Sigma = \nabla\phi|_\Sigma, \quad \mathbf{H}^c|_{t=0} = \mathbf{H}_0, \quad \phi|_{t=0} = \phi_0. \end{cases} \tag{4.1}$$

In the above equations, space and time have been nondimensionalized using a reference length-scale L and the time scale $T_d = \mu\sigma L^2$. Searching for an exponentially decaying solution, $\mathbf{H}^c = \mathbf{H}^c_0 e^{\gamma t}$, leads to an eigenvalue problem. Analytic solutions to this eigenvalue problem are known only for some simple geometries of the conducting domain. In the following, we denote by γ the smallest (obviously real) corresponding eigenvalue.

In this section we consider two types of conducting solids: a sphere and ellipsoids (prolate and oblate).

4.1.1 Ohmic decay in a sphere

We consider a sphere of radius $R = 1$ (i.e., the radius of the sphere is the reference length scale). The ohmic decay in a sphere is a textbook diffusion problem [18]. The theoretical decay-rate is $|\gamma_{\text{th}}| = \pi^2$. The corresponding scalar potential in the nonconducting medium in cylindrical coordinates is the dipolar field $\phi = -z\rho^{-3}J_{3/2}(\pi)e^{-|\gamma_{\text{th}}|t}$ where $\rho = (r^2+z^2)^{1/2}$ (the dipolar moment being aligned with the z-axis). The corresponding magnetic field in

cylindrical coordinates is given by

$$H_r = \sin(\varphi)B_\rho + \cos(\varphi)B_\varphi, \tag{4.2}$$
$$H_z = \cos(\varphi)B_\rho - \sin(\varphi)B_\varphi, \tag{4.3}$$

where $\cos(\varphi) = z/\rho$, $\sin(\varphi) = r/\rho$, and

$$B_\rho = 2e^{-|\gamma_{\rm th}|t}\cos(\varphi)J_{3/2}(\pi\rho)\rho^{-3/2}, \tag{4.4}$$
$$B_\varphi = e^{-|\gamma_{\rm th}|t}\sin(\varphi)(J_{3/2}(\pi\rho) - \pi\rho J_{1/2}(\pi\rho))\rho^{-3/2}. \tag{4.5}$$

The above field is used as the initial condition in our tests. The outer boundary of the nonconducting medium is the sphere of radius $R_v = 10$. We use meshes with meshsizes $h = 1/10,\ 1/40,\ 1/80$ to observe the convergence with respect to the spatial resolution. The time step is taken to be $\Delta t = 10^{-3}$.

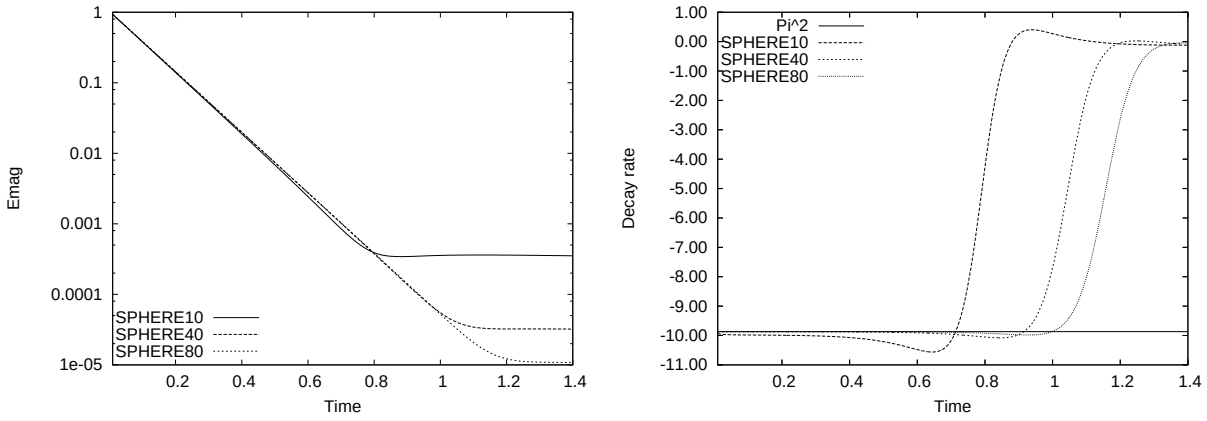

(a) (b)

Figure 2: Ohmic diffusion in a sphere for different mesh sizes $h = 1/10,\ 1/40,\ 1/80$: time evolution of (a) magnetic energy and (b) decay rate of the magnetic energy.

The time evolution of the magnetic energy and its instantaneous decay rate is shown in Figure 2. More precisely, upon setting $E_{\rm mag} = \frac{1}{2}\int_{\Omega_c}\|\mathbf{H}^c\|^2$, we report $E_{\rm mag}$ as a function of time t in Figure 2a and $d\log(E_{\rm mag})/dt$ in Figure 2b. The decay rate reaches a plateau after a few time-steps for the three resolutions considered. The value of the plateau γ is recorded and its absolute value is reported in Table 1.

Note that after eight to ten diffusion times, the computed decay rate increases and finally tends to zero. This is a consequence of problem (4.1) not being well-posed at steady state. As a result, at steady state we obtain a magnetic field whose amplitude is controlled by the divergence of the initial field. Since we use Lagrange interpolants to initialize our computations, the divergence of our initial data is of order $h^{k'}$. This leads to a non-dissipative magnetic energy at steady state. This residual magnetic, denoted by E_{noise}, is reported in Table 1. Observe that E_{noise} goes to zero as $h \to 0$.

h	$\|\gamma\|$	error	t_{noise}	E_{noise}
1/10	9.9921	1.2 %	0.65	3.52 10^{-4}
1/40	9.8741	0.05 %	0.9	3.20 10^{-5}
1/80	9.8686	0.01 %	1	1.01 10^{-5}

Table 1: Ohmic diffusion in a sphere for different mesh sizes h: decay rate of the magnetic energy $|\gamma|$, relative error between $|\gamma|$ and π^2, characteristic time t_{noise} of the end of the exponential decay, level of energy due to discretization errors E_{noise}.

4.1.2 Ohmic decay in an ellipsoid

In order to measure the influence of the conductor geometry, we now study the ohmic decay in ellipsoids. Recall that no analytical expression of the decay-rate is available in this case. Let us denote by a, b, c the semi-axes, with $a = b$ to enforce axisymmetry. We refer to a and c as the half-width and the half-height, respectively. Letting V be the volume of the ellipsoid, the reference lengthscale is defined to satisfy $\frac{4}{3}\pi L^3 = V$, i.e., L is the radius of the sphere having the same volume. Two cases are considered in detail: (1) an 'oblate' spheroid $a = 2$ and $c = 0.25$ and (2) a 'prolate' spheroid $a = 0.75$ and $c = 1.78$. Each ellipsoid is embedded in a nonconducting sphere of radius $R_v = 10$.

The initial magnetic field is chosen to be uniform and parallel to the z-axis. The corresponding magnetic potential in vacuum is $\phi = z$. After $t = 0$, this field is gradually extinguished at Γ_v by enforcing:

$$\phi(t)|_{\Gamma_v} = \frac{z}{1 + (t/t_{\text{ext}})^3}$$

where t_{ext} is the extinction time. Since we expect the decay rate to be of the same order as that of the sphere ($|\gamma_{\text{th}}| \sim \pi^2$), we set $t_{\text{ext}} = 10^{-2}$ and $\Delta t = 5\ 10^{-4}$. This choice guarantees that t_{ext} is significantly smaller than the ohmic diffusion time.

The instantaneous decay-rates of the radial and vertical components of the magnetic field are displayed in Figure 3 for the two ellipsoids and two meshsizes ($h = 1/20,\ 1/40$). After a few time-steps, each decay rate reaches a plateau, then increases and finally tends to zero like in the case of the sphere.

We observe that the decay-rate of the oblate spheroid is about -9.3 and that of the prolate spheroid is about -13.4. In other words by denoting γ_{obl}, γ_{pro}, and γ_{sph} the decay rates of the oblate ellipsoid, the prolate ellipsoid, and the sphere, we have

$$|\gamma_{\text{obl}}| < |\gamma_{\text{sph}}| < |\gamma_{\text{pro}}|.$$

We interprete this result as follows. Since in the sphere the decaying magnetic field is supported by an azimuthal current density that is maximum at $r \simeq 0.9R$, it seems natural that oblateness allows for a larger effective radius for the current and consequently a longer decay time as long as the corresponding reduction of the half-height c does not

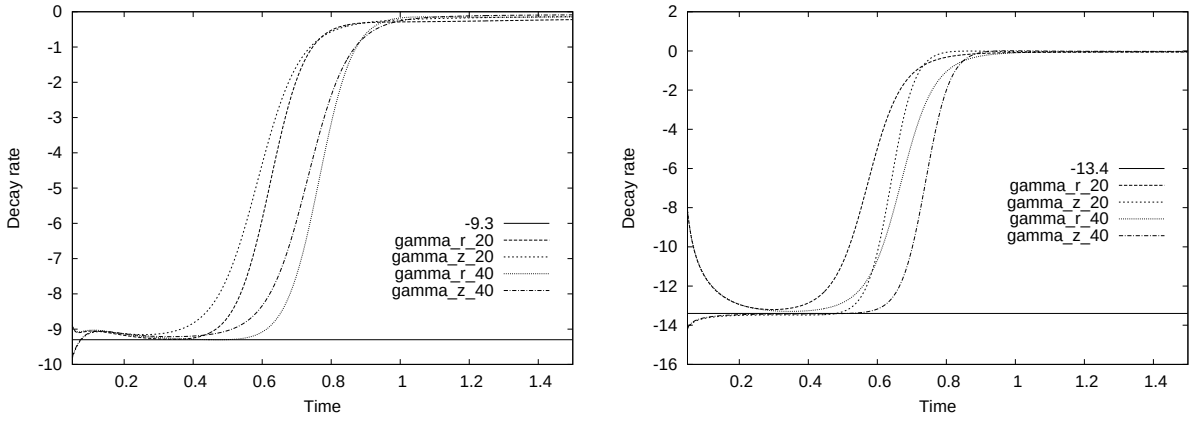

(a) (b)

Figure 3: Ohmic diffusion in two spheroids for different mesh sizes $h = 1/20,\ 1/40$: time evolution of the decay rates for the H_r component γ_r and the H_z component γ_z: (a) oblate spheroid, (b) prolate spheroid.

constrain too much the total current. In conclusion, the absolute value of the decay rate decreases then increases as a goes from 0 to $+\infty$ as shown on Figure 4, i.e., there exists an oblate ellipsoid for $a = 1.5$ with a decay rate whose absolute value is minimum. This curve suggests that the ohmic decay rate of astrophysical objects flattened by rotation may be different from that of similar undeformed objects.

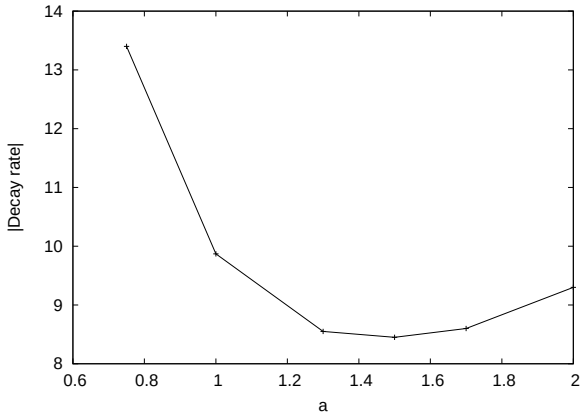

Figure 4: Absolute value of the decay rate as a function of the half-width of the ellipsoid a. The minimum is reached for $a = 1.5$.

4.2 Kinematic dynamo

We now turn our attention to the dynamo action. For the time being we only consider the kinematic dynamo, i.e., that for which the velocity field is prescribed and time-independent. Validation of the kinematic code is a prerequisite for the full nonlinear

dynamo problem, where the Navier-Stokes equations including the Lorentz force are also solved. Henceforth our domain is composed of a solid component of constant conductivity σ_{solid} and a fluid component of constant conductivity σ_{fluid} such that $\sigma_{\text{solid}}/\sigma_{\text{fluid}} = 5$. The problem is described by (2.3) where $\mathbf{u}$ is zero in the solid and $\mathbf{u}$ is prescribed in the fluid. The current $\mathbf{j}^s$ is set to zero everywhere. Letting L be a reference length scale, the time is nondimensionalized with respect to the ohmic decay time, $T_d = \mu\sigma_{\text{fluid}}L^2$. Letting U be a reference velocity scale, we define the magnetic Reynolds number $R_{\text{m}} = \mu\sigma_{\text{fluid}}UL$.

The configuration we want to model is inspired from the so-called Perm device [10, 7]. This experiment aims at generating the dynamo effect in a strongly time-dependent helical flow created in a toroidal channel after impulsively stopping the fast rotating container. Two axisymmetric conducting media whose meridian sections are shown in Figure 5-(a)-(b) are considered. The first case consists of a ring torus (i.e., of circular cross section) hereafter referred to as 'torus'. The reference length scale is chosen so that the nondimensional mean radius of the torus (i.e., the distance between the z-axis and the center of the cross section) is $R = 4$. The nondimensional radius of the circular cross section is $\rho_1 = 1.6$. The inner part of the torus, $0 \leq \rho < \rho_0 = 1.2$, is occupied by the conducting fluid and is referred to as the fluid channel. The outer part of the torus, $\rho_0 < \rho < \rho_1$ is occupied by the conducting solid. The second case consists in a variation of the torus geometry where the conducting domain includes flat equatorial protuberances. The second setting is hereafter referred to as the 'Perm' case, since it is closer to the real experimental geometry.

The flow velocity is assumed to have a uniform azimuthal component that we henceforth denote by U_{a}. The reference velocity U is chosen to be $U = U_{\text{a}}\rho_0$ so that the magnetic Reynolds number can be rewritten as $R_{\text{m}} = \mu\sigma_{\text{fluid}}U_{\text{a}}(\rho_0 L)$. The non-dimensional helical flow in the fluid channel is then defined in cylindrical coordinates by

$$u_r = -\chi\frac{1}{\rho_0}\frac{Rz}{\rho_0 r}, \quad u_\theta = \frac{1}{\rho_0}, \quad u_z = \chi\frac{1}{\rho_0}\frac{R(r-R)}{\rho_0 r} \tag{4.6}$$

where χ is a constant hereafter referred to as the poloidal to toroidal velocity ratio. We choose $\chi = 1$ as in [7], where the case of the straight cylinder ($R = \infty$) is studied in details. Since the flow $\mathbf{u}$ is axisymmetric, the term $\nabla\times(\mathbf{u}\times\mathbf{H}^c)$ cannot transfer energy between the azimuthal modes of $\mathbf{H}^c$, i.e., the azimuthal modes are uncoupled; therefore, the initial magnetic field in the conductor is set to contain all the azimuthal modes that we want to test. To achieve this goal, the simulations are initialized as follows. The magnetic field is set to zero at $t = 0$, then we impose an azimuthal current on the modes $m \in \{1, \ldots, 5\}$ for $0 < t \leq t_{\text{ext}} = 0.01$, i.e., after t_{ext} the current is set to zero.

The magnetic energy on every mode is recorded as a function of time for various magnetic Reynolds numbers $R_{\text{m}} \in [10, 30]$. Figure 6(a) shows the magnetic energy as a function of time for the 'Perm' case at $R_{\text{m}} = 30$. After thorough investigations, we have found that $m = 3$ is the critical mode corresponding to the lowest critical magnetic Reynolds number in both the 'Perm' and the 'Torus' cases. More precisely we have

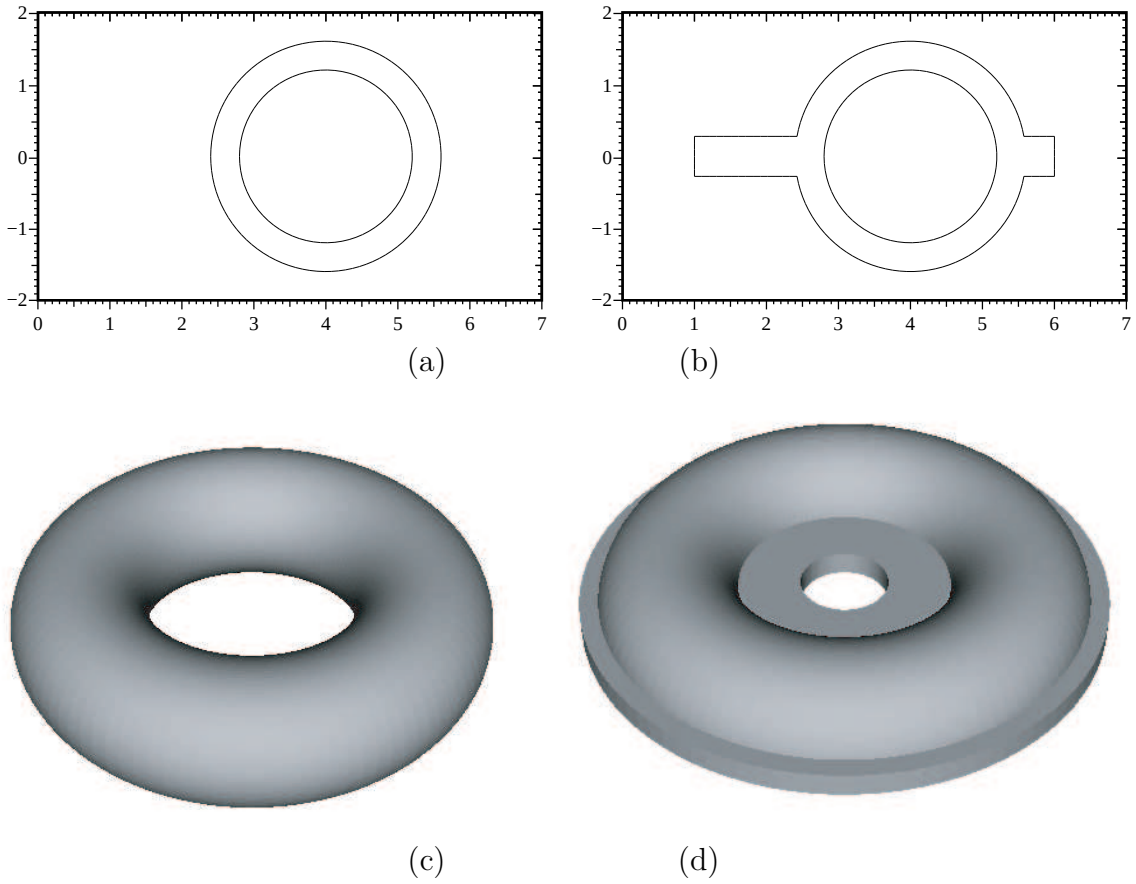

Figure 5: Schematic representation of the two tori configurations. (a) and (b) are cross sections in the meridian plane; (c) and (d) are three-dimensional renderings. (a)–(c) correspond to the 'Torus' case and (b)–(d) to the 'Perm' case.

determined $R_{\rm m}^c(\text{Perm}) \simeq 16 \pm 0.5$ and $R_{\rm m}^c(\text{torus}) \simeq 17.5 \pm 0.5$ (see Figure 6(b)).

The above thresholds are lower than the threshold $R_{\rm m}^c = 22.8$ found in [7] with the ratio $(\rho_1 - \rho_0)/\rho_0 = 0.33$ in the case of a straight pipe (i.e., a torus with $R/\rho_0 \to \infty$). Curvature effects seem to be solely responsible for this difference, since all cases have a conducting solid envelope with the same radius and the same fivefold increase of conductivity. We show in Figure 7 the H_θ-component of the unstable mode for the 'Perm' case at $R_{\rm m} = 17 > R_{\rm m}^c(\text{Perm})$. Observe that the support of this unstable eigenmode is localized close to $\rho \approx \rho_0$, i.e., in the region of maximum shear. This eigenmode has a double helix shape and has the same helicity sign as that of the velocity field. By recording the time evolution of the magnetic field at various fixed points in the fluid domain, we observe that each signal is composed of a growing exponential envelope and of a periodic component. At every point, we observe that the period of the periodic component is $T_{\rm period} \approx 4$ related to the angular frequency $\omega = 2\pi/T_{\rm period}$. The phase speed associated with an $m = 3$ mode is by definition $\frac{\omega}{3}$. By taking two snapshots of the magnetic field at two times t_1, t_2 such that

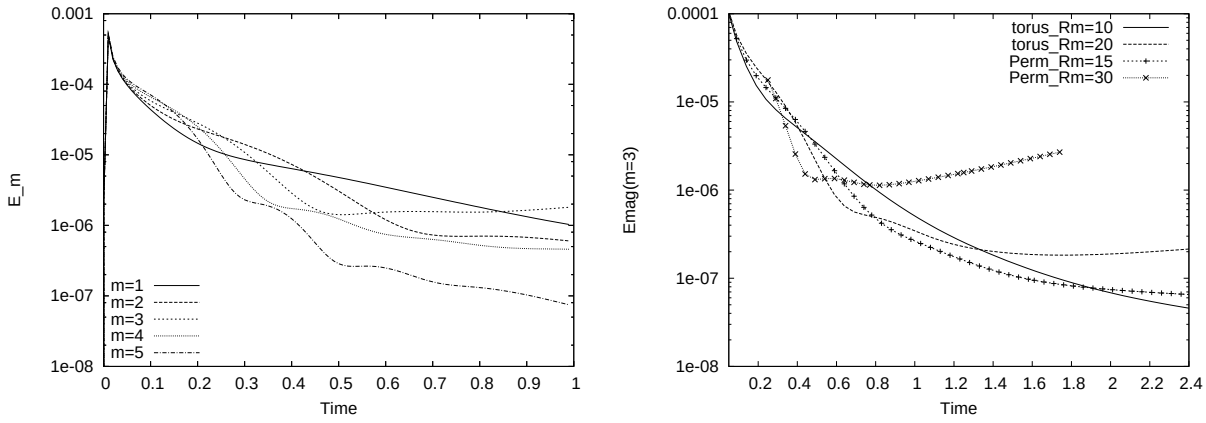

(a) (b)

Figure 6: Time evolution of the magnetic energy: (a) at $R_{\rm m} = 30$ for $m \in \{1, \cdots, 5\}$ for the Perm case; (b) for $m = 3$ at different $R_{\rm m}$ for the two cases: 'torus', 'Perm'.

$t_2 - t_1 = \frac{1}{4} T_{\rm period}$, the angular displacement between these two snapshots should be

$$\frac{\omega}{3} \frac{1}{4} T_{\rm period} \approx \frac{1}{6} \pi = 30^o,$$

which is exactly the angular displacement that is observed in Figures 7 (a) and (b).

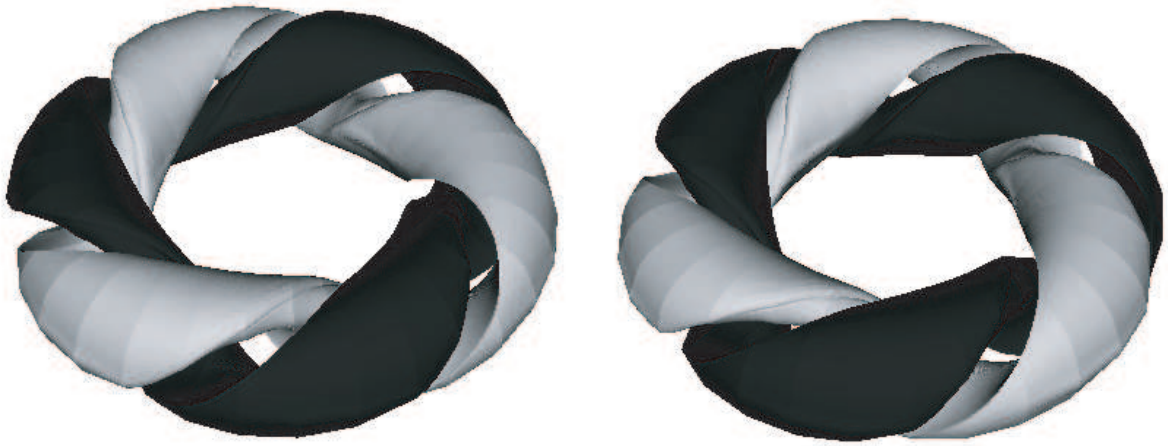

(a) (b)

Figure 7: Perm dynamo at $R_{\rm m} = 17$: iso-surfaces of the H_θ component of the $m = 3$ mode; $H_\theta = 25\%$ of the minimum value (black) and $H_\theta = 25\%$ of the maximum value (white) at (a) $t = 1$ and (b) $t = 2 \simeq 1 + \frac{1}{4} T_{\rm period}$ where $T_{\rm period}$ is the period.

In the above discussion we have assumed that the flow is steady. In the Perm experiment, this is definitely not the case since high magnetic Reynolds numbers are generated

by impulsively braking the container. Before doing simulations with time-dependent flows, which could be done in principle with our code, it is thus wise to verify that the time interval where $R_{\rm m}$ stays above critical (estimated from experiments using water models) is indeed larger than the dynamo growth time $T_{\rm growth}$. Let us consider the growth time at $R_{\rm m} = 30$, i.e. about twice the critical value. Below $R_{\rm m} = 30$ we have found that the real part of the growth rate γ is quasi-linear with respect to $R_{\rm m}$: $\Re(\gamma) = \alpha(R_{\rm m}/R_{\rm m}^c - 1)$ with $\alpha \simeq 2.24$. At $R_{\rm m} = 30$, the characteristic growth time is thus about $T_{\rm growth} \approx T_d/(\alpha(30/16-1)) \approx 0.5T_d$, which must be compared with the life time of the flow at $R_{\rm m} \geq 30$, which is about ten rotation periods acccording to [10], i.e., $T_{\rm flow} = 10(2\pi R)/U_{\rm a}$. This leads to the following estimation

$$\frac{T_{\rm flow}}{T_{\rm growth}} \approx \frac{20\pi R}{0.5\mu\sigma_{\rm fluid}L^2U_{\rm a}} = \frac{20\pi\rho_0 RL^{-1}}{0.5R_{\rm m}} \approx 20$$

which is hoped to be sufficient for the dynamo action to settle in the Perm experiment. This conjecture however deserves more detailed examination by taking into account the effective time history of the magnetic Reynolds number.

5 Conclusion

The Maxwell equations in the MHD limit in heterogeneous domains are solved by using the magnetic field $\mathbf{H}^c$ in the conducting regions and the magnetic scalar potential ϕ in the nonconducting regions. We use Lagrange finite elements and enforce continuities across interfaces using an interior penalty technique à la Nitsche/Dupont–Douglas. The method is shown to be stable and convergent. In axisymmetric domains, finite elements are used in the meridian plane and Fourier expansions in the azimuthal direction. Lagrange elements of degree 1 to approximate $\mathbf{H}^c$ in the conducting region and Lagrange elements of degree 2 to approximate ϕ in the nonconducting region lead to $\mathcal{O}(h^{3/2})$ error in the L^2-norm of the magnetic field.

Our algorithm is limited to simply connected nonconducting domains for the time being or tori with zero net current. Actually, using a scalar potential ϕ to represent the external magnetic field is possible as soon as the circulation of the magnetic field vanishes around every closed path in the vacuum. This is indeed the case for time-dependent dynamo computations starting with a potential initial magnetic field. In this case the induced fields and currents are on mode $m \neq 0$, and the net current on mode $m = 0$ stays equal to zero. Thus, although the present algorithm is not yet capable of simulating tokamak MHD problems (which have net toroidal currents), it can be used for simulating conducting flows in a torus like we did for the Perm device [7]. Note also that the algorithm can deal with spatial distributions for σ and μ and that opens new perspectives for studying more realistic configurations.

We have studied Ohmic decay in axisymmetric compact conducting regions such as a sphere and ellipsoids. The algorithm may also be directly used for a much larger variety of applications of practical interest, after proper selection of the boundary conditions

and adapting the mesh to the topology of the problem. For example, computations of induction in a rotating infinite or finite cylinder are reported in [17]. This code is also able to describe the kinematic dynamo acting in axisymmetric finite containers as presented in §4.2, including conductivity jumps.

After coupling the present code with its FEM hydrodynamical counterpart, which is now available, we will be ready to examine nonlinear MHD phenomena occurring in realistic configurations.

Acknowledgments

We are deeply grateful to the organizers of the summer MHD program 2005 at Université Libre de Bruxelles, D. Carati, S. Kassinos and B. Knaepen where part of the runs was performed. We acknowledge fruitful discussions with W. Dobler, P. Frick and R. Stepanov. R.L. is thankful to Texas A&M University for supporting him in 2005.

REFERENCES

[1] A. Alonso. A mathematical justification of the low-frequency heterogeneous time-harmonic Maxwell equations. *Math. Models Methods Appl. Sci.*, 9(3):475–489, 1999.

[2] A. Bossavit. Magnetostatic problems in multiply connected regions: Some properties of the curl operators. *Proc. Inst. Elec. Eng.*, 135:179–187, 1988.

[3] A. Bossavit. The computation of eddy-currents, in dimension 3, by using mixed finite elements and boundary elements in association. *Math. Comput. Modelling*, 15(3-5):33–42, 1991.

[4] A. Bossavit. *Computational Electromagnetism, Variational Formulations, Complementary, Edge Elements*, volume 2 of *Electromagnetism*. Academic Press, 1998.

[5] B. Cockburn and C.W. Shu. The local discontinuous Galerkin method for time-dependent convection-diffusion systems. *SIAM J. Numer. Anal.*, 35:2440–2463, 1998.

[6] M. Costabel. A coercive bilinear form for Maxwell's equations. *J. Math. Anal. Appl.*, 157(2):527–541, 1991.

[7] W. Dobler, P. Frick, and R. Stepanov. Screw dynamo in a time-dependent pipe flow. *Phys. Rev. E*, 67:056309, 2003.

[8] J. Douglas Jr. and T. Dupont. *Interior Penalty Procedures for Elliptic and Parabolic Galerkin Methods*, volume 58 of *Lecture Notes in Physics*. Springer-Verlag, Berlin, 1976.

[9] P. Dular and C. Geuzaine. Modeling of thin insulating layers with 3D magnetodynamic formulations. *IEEE Transactions on magnetics*, 39:1139–1142, 2003.

[10] P. Frick, V. Noskov, S. Denisov, S. Khripchenko, D. Sokoloff, R. Stepanov, and A. Sukhanovsky. Non-stationary screw flow in a toroidal channel: way to a laboratory dynamo experiment. *Magnetohydrodynamics*, 38(1-2):143–162, 2002.

[11] J.-L. Guermond, R. Laguerre, J. Léorat, and C. Nore. An Interior Penalty Galerkin Method for the MHD equations in heterogeneous domains. *J. Comput. Phys.*, 2006. Submitted.

[12] J.-L. Guermond, J. Léorat, and C. Nore. A new finite element method for magneto-dynamical problems: two-dimensional results. *Eur. J. Mech./Fluids*, 22:555–579, 2003.

[13] J.-L. Guermond and P.D. Minev. Mixed finite element approximation of an MHD problem involving conducting and insulating regions: the 2D case. *Modél. Math. Anal. Numér. (M2AN)*, 36(3):517–536, 2002.

[14] J.-L. Guermond and P.D. Minev. Mixed finite element approximation of an MHD problem involving conducting and insulating regions: the 3D case. *Numer. Methods Partial Differential Eq.*, 19(6):709–731, 2003.

[15] A. B. Iskakov, S. Descombes, and E. Dormy. An integro-differential formulation for magnetic induction in bounded domains: boundary element-finite volume method. *J. Comput. Phys.*, 197(2):540–554, 2004.

[16] J. Zou K. H. Chan, K. Zhang and G. Schubert. A non-linear, 3-D spherical α^2 dynamo using a finite element method. *Physics of the Earth and Planetary Interiors*, 128:35–50, 2001.

[17] R. Laguerre, C. Nore J. Léorat, and J.-L. Guermond. Induction effects in isolated axisymmetric conductors using a new finite element method. In D. Carati and B. Knaepen, editors, *Proceedings of the Bruxelles ULB MHD Workshop*, Bruxelles, July 2005 2006.

[18] H.K. Moffatt. *Magnetic Field Generation in Electrically Conducting Fluids*. Cambridge Monographs on Mechanics and Applied Mathematics. Cambridge University Press, Cambridge, 1978.

[19] J. Nitsche. Über ein Variationsprinzip zur Lösung von Dirichlet-Problemen bei Verwendung von Teilräumen, die keinen Randbedingungen unterworfen sind. *Abh. Math. Sem. Univ. Hamburg*, 36:9–15, 1971.

[20] Ilaria Perugia and Dominik Schötzau. The *hp*-local discontinuous Galerkin method for low-frequency time-harmonic Maxwell equations. *Math. Comp.*, 72(243):1179–1214 (electronic), 2003.